PROGRESS IN APPLIED SCIENCE AND TECHNOLOGY
Faculty of Science and Technology
Rajamangala University of Technology Thanyaburi
Prog Appl Sci Tech. 2023; 13(3):27-34
ISSN (Print): 2730-3012
ISSN (Online): 2730-3020
https://ph02.tci-thaijo.org/index.php/past

Research Article

Received: June 23, 2023
Revised: August 14, 2023
Accepted: August 25, 2023

DOI: 10.60101/past.2023.250546

Zinc Oxide Nanowall Networks Growth on Indium Tin Oxide Substrates in an Oxygen Atmosphere and Magnetic Field via the Sparking Process

Chalao Wongsaeng[1,3*] and Roongroj Kamanja[2,3]
[1] *Department of Science, Faculty of Sciences and Agricultural Technology, Rajamangala University of Technology Lanna Tak, Tak 63000, Thailand*
[2] *Department of Electrical Engineering, Faculty of Engineering, Rajamangala University of Technology Lanna Tak, Tak 63000, Thailand*
[3] *Advanced Physics Research Laboratory, Department of Science, Faculty of Sciences and Agricultural Technology, Rajamangala University of Technology Lanna Tak, Tak 63000, Thailand*
*E-mail: chalao2515@rmutl.ac.th

Abstract

A zinc oxide nanowall (ZnO NW) network was grown on an indium tin oxide (ITO) surface using the sparking process at a breakdown voltage. This process involved the growth of materials through chemical vapor deposition constituted an integral part of this procedure, four pairs of pure zinc wire electrodes in a flowing oxygen atmosphere, with a perpendicular magnetic field applied downward onto the ITO surface. It was observed that the growth of the ZnO NW network on the ITO surface is accompanied by an increase in both the size of individual ZnO NW and the volume of each ZnO NW cluster, which correlates with the number of coating. The transmittance measurements of the glass/ITO/ZnO NW network substrates indicate the successful formation of the nanostructure and the attainment of enhanced crystallinity.

Keywords: Zinc Oxide Nanowall Network, Breakdown Voltage, Chemical Vapor Deposition, Transmittance

1. Introduction

Numerous researchers are currently investigating the synthesis process of zinc oxide nanoparticle (ZnO NP) films for various applications, such as sensor materials (1-4), transport layers in solar cells (5, 6), and hydrogen storage devices (7, 8). Zinc oxide nanoparticles come in various shapes, including nanowalls (NW) (1-4, 6, 8-15), nanorods (16, 17), and nanowires (12), each with distinct properties. Chemical methods, such as chemical bath deposition and hydrothermal processes, are often employed to synthesize ZnO NPs from precursor chemical compounds (1, 9-11).

The objective of this research is to cultivate ZnO nanowalls (NWs) on an indium tin oxide (ITO)/glass substrate or an ITO substrate by utilizing sparking electrodes in an oxygen atmosphere and a magnetic field. The electrical method has been utilized to synthesize nanomaterials such as ZnO nanoparticles, as in the previous works, due to its simplicity (18-19). The breakdown voltage of the medium between electrodes can be reduced by adding the oxygen atmosphere (20). In this study, we utilized chemical vapor deposition (CVD) growth via sparking electrodes consisting of four pairs of zinc wires to fabricate the ZnO NW network and

subsequently examined its transmittance properties. The growth of the ZnO NW network on the ITO substrate holds potential for utilization as the electron transport layer (ETL) in solar cells.

2. Materials and Experiment

The sparking apparatus, as depicted in Figure 3a (Scan XY-36 Model, Nano Generation Co. Ltd.), comprises four pairs of electrodes and sparks with a high DC voltage (approximately 3 kV in air). During the operation of the sparking apparatus, the sparking head scanned forward and backward along the X-direction, while the substrate holder moved backward along the Y-direction to coat zinc particles onto the substrate. The material subjected to the process is pure zinc wires (diameter 0.38 mm, purity 99.97%, Advent Research Material Ltd.), which undergo sparking or electron discharge at a breakdown voltage of the insulators (or the medium) (19, 20). This results in particles coating the ITO/glass substrate at a spark coating rate of 14.4 mm^2/min. The gap between electrodes in each pair was set at 1.0 mm; the distances between pairs were set at 10.0 mm for the shortest, 14.0 mm for the longest; and the working distance (WD) between the electrode tips and the surface of ITO/glass substrate was defined as 1.0 mm. Additionally, a magnetic field was established by placing a permanent magnetic coin array below the substrate holder, with the south magnetic pole positioned at the top. Each magnetic coin has diameter 10.00 mm. The magnetic field strength at the electrode-tip position measured 37.2 mT (measured using a Teslameter in a direct field, PHYWE).

The ITO substrates (cut to a size of 10.0 mm x 10.0 mm with an average surface resistance of 2.20 Ω/mm) underwent cleaning in a 99.5% acetone solution through ultrasonic cleaning at a frequency of 40 kHz. Subsequently, they were dried by annealing in an electric oven at 110°C for 30 minutes. The zinc wires and substrates were positioned on the wire holder and substrate holder, respectively (Figure 3a). Pure oxygen (O_2, U.H.P. 99.999%) was chosen as the medium for sparking. It entered the spark chamber (18 x 18 x 18 cm^3) at a flow rate of 100 cm^3/min and exited through an outlet connected to a long tube (diameter approximately 5.0 mm, length around 5 m) leading to the fume hood (with a suction rate of 1000 m^3/h, Green Tech Plus).

The sparking process was employed to coat zinc particles onto the ITO surfaces, with a varying number of coatings (0, 4, 6, 8, and 10 times). Subsequently, the products were characterized to determine oxide type and crystallinity using field emission scanning electron microscopy (FE-SEM, JEOL JSM-6335F) and X-ray photoelectron spectroscopy (XPS, AXIS Ultra DLD).

A solar simulator was created using a PHILIPS PAR38EC lamp as an artificial solar radiation source. The spectrum or artificial radiation power density of this source was measured using a photoluminescence spectrometer (PL, Avantes), and its corresponding spectrum is depicted on the vertical axis (left) of Figure 4a. This spectrum corresponds to the spectral irradiance-global tilt (W/m^2/nm) (right vertical axis) at the solar constant 1.5, based on the ASTM G173-03 reference spectra derived from SMARTS v.2.9.2 (21).

The inset in Figure 4c presents measurements of solar energy density distribution at the same level position of 45.0 cm, where data from several points within the 2.50 cm x 2.50 cm area were illustrated in a 3D bar chart. At the position of the substrate holder, which is located 45.0 cm from the lamp, the average radiation power density (wavelength range 400 - 700 nm) was quantified as 1000 W/m^2 (or 100%) when no sample was present. The effective entrance area for the reaction was approximately 38.5 mm^2 (or diameter 7.0 mm) for solar power transmission through the solar power meter. Subsequently, the artificial light was made to pass through samples with triple layers of glass/ITO/ZnO NW network, where the ZnO NW network had undergone spark coating 0, 4, 6, 8, and 10 times. The transmittances (%) of artificial solar power densities passing through each samples was measured using a solar power meter (SM206-SOLAR, Bestone Measuring Instruments). These samples included Glass/ITO (uncoated), and Glass/ITO/ZnO with varying thicknesses of ZnO (coated 4, 6, 8, and 10 times).

3. Results and Discussion

Figures 1a - 1d show FE-SEM images of the sponge-like structures which typically called that ZnO nanowall (NW) networks (1-4, 6, 8-15), grew on ITO surfaces in X5000 magnification by sparking process of four pairs

of positive-negative electrodes of zinc wires in an oxygen atmosphere and magnetic field for number of coatings 4, 6, 8, and 10 times, respectively. It was found that sizes and amount of the ZnO NWs increased with increasing the number of spark coatings with an O_2 flow of 100 cm^3/min and the magnetic field vertically downward. The average thicknesses of the ZnO NW networks in Figures 1a - 1d are 409, 523, 603, and 1009 nm, respectively measured using the software Image J (1.54d). It was noticed that the increasing of the film thicknesses of the ZnO NW network is not linear. This result is expected from the crystallinity of ZnO NW structure under the CVD process (8, 22-24), the depend on the oxygen flow rate. In terms of the size of ZnO NWs, the volume of each ZnO NW cluster increased as the number of coating increased, ~1.1 $\times 10^7$ nm^3, ~1.7 $\times 10^7$ nm^3 and ~1.2 $\times 10^8$ nm^3, for 4, 6, and 10 times, respectively. Each orange circle, depicted in Figure 1a and 1b, defines a cluster of ZnO NWs. It was shown that the number density of ZnO NWs cluster grew on the ITO surface decreased with increasing number of coatings. The morphology shown in Figure 1c looked quite different from that of 1b and 1d. It was expected that there were unexpected phenomena that happened to this sample.

The XPS spectra of the samples in Figures 2a - 2c show that the films formed on ITO are ZnO. Figure 2a displays a high intensity XPS peak indicating the electron load from the main components of ZnO, namely zinc (Zn) and oxygen (O), at a binding energy range of 0 - 1200 eV. The Zinc within ZnO exhibits two distinct binding energies: 1021.7 and 1044.7 eV, which are higher than that of oxygen with a binding energy of 531.7 eV. The asymmetric O 1s peak (Figure 2c) can be divided into four subpeaks at 534.035, 533.025, 531.979, and 530.710 eV. These values can be analyzed to correspond to their O species (25). Comparing these XPS peaks with those of pure zinc wire (Figure 2d), it becomes evident that the XPS peaks of zinc atoms have slightly shifted binding energies, measured at 1022.1 and 1045.2 eV. This observation suggests that the sparking process, under the conditions of this research, provides insights into the oxidation state of the metal (23, 26).

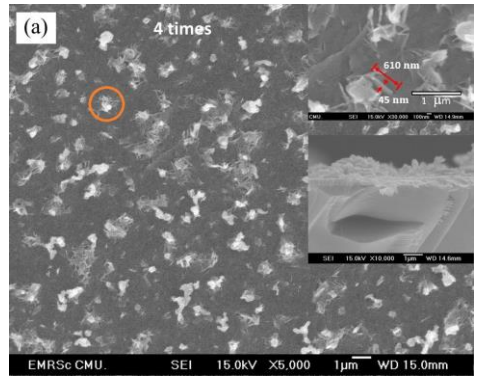

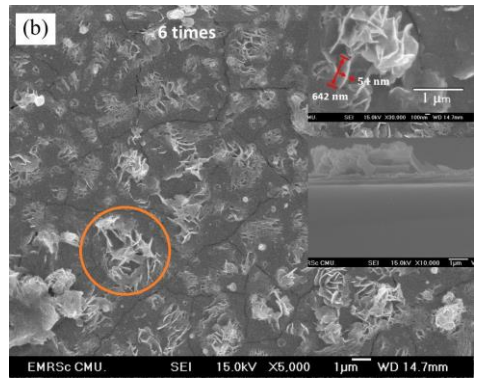

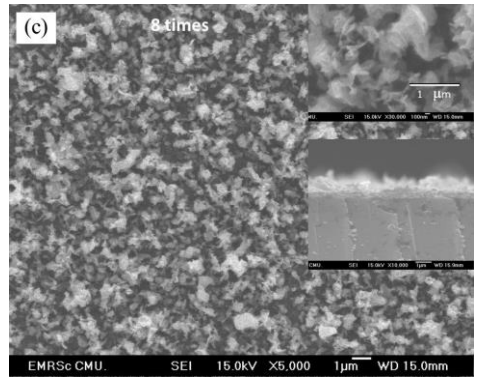

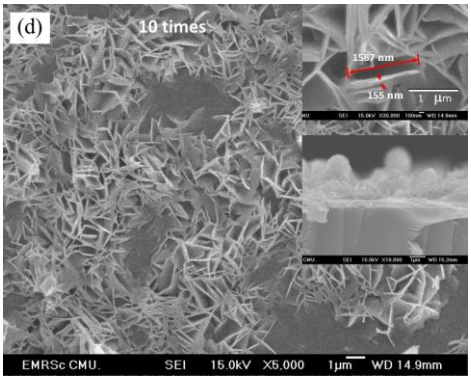

Figure 1 (a) - (d) FE-SEM images of ZnO NW networks grew on ITO surfaces by sparking process of four pairs of zinc wire electrodes in an oxygen atmosphere and a magnetic field for number of coatings 4, 6, 8, and 10 times. Upper and lower insets in figures (a) to (d) show the top view images at X30000 magnification and the cross-sectional view images at X10000 magnification, respectively. The orange circles in the figures (a) and (b) were depicted to define a cluster of ZnO NWs.

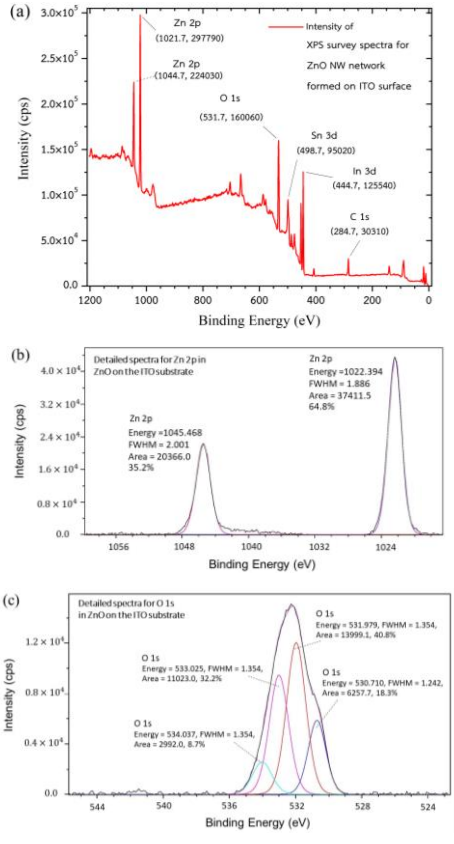

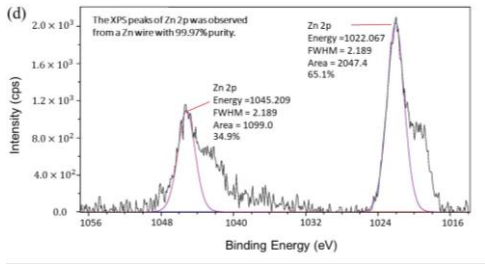

Figure 2 (a) XPS survey spectra of ZnO NW networks grew on ITO surfaces. (b) - (c) Detailed spectra for Zn 2p, and O 1s, respectively. (d) XPS spectra of purity zinc wire.

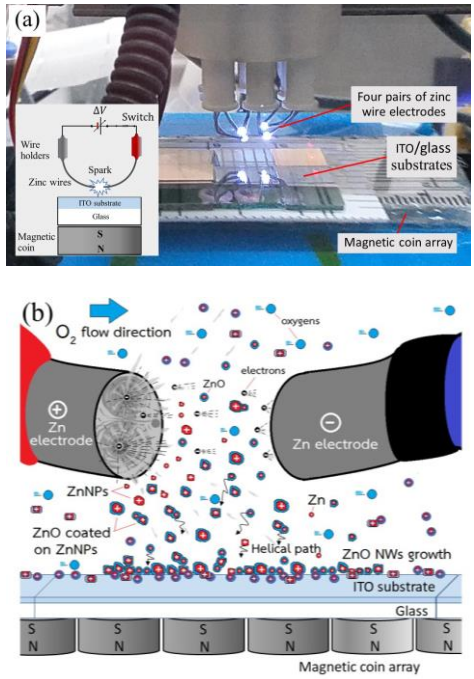

Figure 3 (a) A photograph of the sparking electrodes has four pairs of positive-negative zinc wires as sparking tips. It is being sparked in an oxygen atmosphere and a magnetic field. The inset shows a schematic diagram of a sparking apparatus with one-pair of electrodes, an ITO substrate and a magnetic coin array. (b) A schematic diagram of ZnO NW growth by the sparking process.

Figure 3a illustrates the sparking of four pairs of zinc wire electrodes to generate zinc feedstock on the ITO substrates within an O_2 atmosphere flow of 100 cm³/min. The electrical

conduction of the O_2 medium between the tips of the zinc electrodes occurred when the electric field between the tips exceeded the dielectric strength of the medium. The breakdown voltage of the medium was employed to determine the electric field strength of sparking. These two quantities were correlated using the following equation: $E = \Delta V/d$, where d represents a small perpendicular distance between two equipotential surfaces, and E signifies the electric field strength, which remains nearly constant over this limited distance. ΔV denotes the potential difference between the equipotential surfaces (19, 20, 27).

Subsequently, the charge particles, encompassing electrons and ions, underwent continuous acceleration described by $a = F_E/m = qE/m$. Here, a symbolizes acceleration (m/s²), F_E stands for electric force (N), m denotes the mass of the charge particle (kg), and q represents the particle's charge (C). The sparking bombardment of high-energy electrons and ions caused the zinc tips of these electrodes to melt within the O_2 atmosphere, resulting in the creation of a plasma consisting of zinc atoms, oxygen atoms, secondary particles adjacent to the ITO surface, and high temperature.

Figure 3b provides a schematic diagram illustrating the growth of the ZnO NW network through the sparking process within an O_2 atmosphere, forming the nanostructure. The interaction of these particles could lead to the creation of NWs and NW networks, explained through the CVD process (24, 28-30). Within the stagnant boundary layer adjacent to the ITO substrate's surface, zinc atoms and oxygen atoms engage in diffusion and interaction at the gas-solid interface, resulting in the formation of ZnO molecules and ZnO NW networks on the heated ITO substrates.

Due to the incorporation of the magnetic coin array as part of the substrate holder, with the south magnetic pole positioned at the top, a magnetic field is created, oriented downward and perpendicular to the ITO surfaces. This magnetic field interacts with the charged particles in motion (such as oxygen ions, zinc atoms, and secondary particles), as described by the Lorentz force formula, $\vec{F}_B = q\vec{v} \times \vec{B}$, where $\vec{F}_B$ represents magnetic force (N), q signifies the particle's charge (C), $\vec{v}$ denotes the particle's velocity (m/s), and $\vec{B}$ signifies the magnetic field (T). For example, the helical path of a Zn ion motion downward onto the ITO surface if the motion direction of the Zn ion moves across the z-direction magnetic field with angles between them more than 0° and less than 90°, as shown in Figure 3b.

From the earlier observations in Figures 1a and 1b, ZnO NWs initially grew on the ITO substrate as small clusters. The number density of ZnO NWs cluster decreased with an increasing number of coatings. This structural formation was influenced by the Lorentz force or the magnetic field distribution of the magnetic coin array and the distances between the four pairs of zinc wire electrodes. There is evidence suggesting that the magnetic field altered certain properties within the nanostructures, including the band gap energy (18, 31).

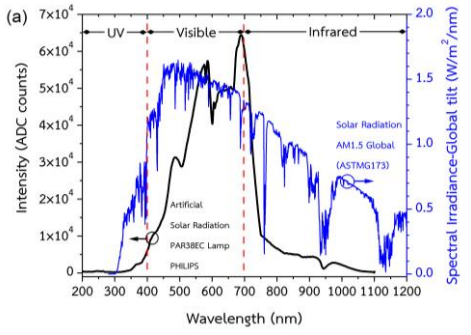

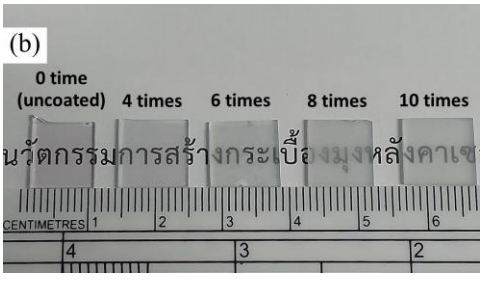

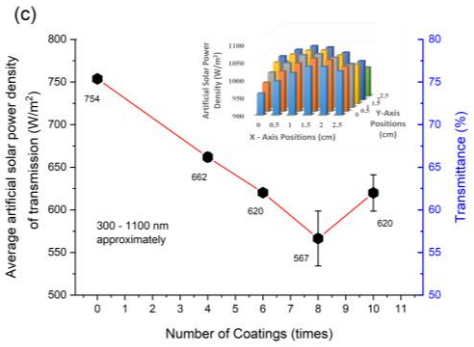

Figure 4 (a) Plot with two vertical axes: intensity (ADC counts) of artificial solar radiation (left) and spectral irradiance-global tilt (right) versus wavelength (21). (b) Photographic images of ZnO NWs formed on ITO substrates with spark coatings 0, 4, 6, 8, and 10 times, respectively. (c) Plot with two vertical axes: the average artificial solar power density of transmission (left) and the transmittance (right) pass through the glass/ZnO NW network versus number of coatings. The inset shows the distribution of artificial solar density onto the test area.

The outcomes of these measurements (Figure 4c) for the average artificial solar power density of transmission are as follows: 754, 662, 620, 567, and 620 W/m² (left) corresponding to transmittances of 75.4%, 66.2%, 62.0%, 56.7%, and 62.0% (right), respectively. Notably, the transmittances of the samples decreased with 4, 6, and 8 spark coatings. However, with 10 spark coatings in relation to 6 or 8 coatings, the transmittance sequences exhibited a re-increasing trend. This trend was attributed to the effect of ten spark coatings, which resulted in the complete formation of the ZnO NW network's nanostructure and higher crystallinity within the sponge-like structure of the ZnO NWs covering the substrate (15, 22, 23). This outcome aligns with the increased transparency observed in samples with 10 spark coatings, as presented in Figure 4b.

To establish an effective electron transport layer in solar cells, further comprehensive studies are required to harness the full potential of the complete nanostructure of the ZnO NW network achieved through the sparking process.

4. Conclusions

The sparking apparatus, equipped with four pairs of zinc wire electrodes, initiates sparking at high DC voltages. This process, occurring at the breakdown voltage within an oxygen atmosphere and aided by a magnetic field positioned at the electrode-tip location, results in the coating of particles onto ITO substrates, ultimately forming the ZnO NW network on ITO surfaces. This structural configuration was verified through FE-SEM images, and the XPS peaks of Zn 2p from the sparking product displayed a slight shift compared to those of pure zinc wire.

The ZnO NW product (or ZnO NW network) can be described through the CVD process. This involves the diffusion and interaction of zinc atoms and oxygen atoms at the gas-solid interface on the ITO substrates. Notably, the number density of ZnO NWs cluster grown on the ITO surface diminishes with an increase in the number of coatings. This structural formation appears to be influenced by the distribution of the magnetic field and the spacing between electrodes.

Conducting transmittance tests wherein artificial sunlight passes through samples consisting of glass/ITO/ZnO NW network, measured using a solar power meter, reveals that after ten times of sparking, the structure attains completeness within the nanostructure and displays higher crystallinity.

Acknowledgements

The authors express their gratitude to the Electricity Generating Authority of Thailand (EGAT), Bhumibol Dam, for their financial support. Special thanks are extended to Rajamangala University of Technology Lanna Tak for providing essential utilities. The authors would also like to acknowledge the dedicated scientists and technicians at Chiang Mai University: Mr. Ekkapong Kuntarak, Mr. Thawatchai Sakhon, Mr. Chanvit Sriprom, and Ms. Tanyakarn Phutayanon; and at Rajamangala University of Technology Lanna Tak, Mr. Songsaeng Wattanayungyuen. Heartfelt appreciation is offered to Assoc. Prof. Dr. Pisith Singjai, Mr. Phongthep Janpoom, Dr. Samor Boonphan, Ms. Natakamon Koontasing, and Dr. Posak Tippo for their valuable consultations.

Additionally, a special note of thanks goes to Asst. Prof. Dr. Sawitri Suwanaroa for her assistance in improving the language aspects at Rajamangala University of Technology Lanna Tak.

Declaration of conflicting interests

The authors declared that they have no conflicts of interest in the research, authorship, and this article's publication.

References

1. Feng Z, Rafique S, Cai Y, Han L, Huang M-C, Zhao H. ZnO Nanowall Networks for Sensor Devices: From Hydrothermal Synthesis to Device Demonstration. ECS J Solid State Sci 2018;7(7):Q3114.
2. Bruno E, Strano V, Mirabella S, Donato N, Leonardi SG, Neri G. Comparison of the Sensing Properties of ZnO Nanowalls-Based Sensors toward Low Concentrations of CO and NO2. Chemosensors. 2017;5(3):20
3. Wang X, Ding Y, Li Z, Song J, Wang ZL. Single-Crystal Mesoporous ZnO Thin Films Composed of Nanowalls. J Phys Chem C. 2009;113(5):1791-4.
4. Yu L, Wei J, Luo Y, Tao Y, Lei M, Fan X, et al. Dependence of Al3+ on the growth mechanism of vertical standing ZnO nanowalls and their NO2 gas sensing properties. Sensors Actuators B: Chem. 2014;204:96-101.
5. Lin L, Jiang L, Li P, Fan B, Qiu Y. A modeled perovskite solar cell structure with a Cu2O hole-transporting layer enabling over 20% efficiency by low-cost low-temperature processing. J Phys Chem Solids. 2019;124:205-11.
6. Liang Z, Gao R, Lan J-L, Wiranwetchayan O, Zhang Q, Li C, et al. Growth of vertically aligned ZnO nanowalls for inverted polymer solar cells. Sol. Energy Mater Sol. Cells. 2013;117:34-40.
7. Saravanakumar B, Kim S-J. Growth of 2D ZnO Nanowall for Energy Harvesting Application. J Phys Chem C. 2014;118(17):8831-6.
8. Kim S-W, Fujita S, Yi M-S, Yoon DH. Catalyst-free synthesis of ZnO nanowall networks on Si3N4⁄Si substrates by metalorganic chemical vapor deposition. Appl Phys Lett. 2006;88(25):253114.
9. Jiang B-C, Yang S-H. Nickel-Doped ZnO Nanowalls with Enhanced Electron Transport Ability for Electrochemical Water Splitting. Nanomater (Basel, Switzerland). 2021;11(8).
10. Jin C, Li J, Wang J, Han S, Wang Z, Sun Q. Cross-Linked ZnO Nanowalls Immobilized onto Bamboo Surface and Their Use as Recyclable Photocatalysts. Guo C, editor. J Nanomater. 2014;2014:687350.
11. Pellegrino D, Franzò G, Strano V, Mirabella S, Bruno E. Improved Synthesis of ZnO Nanowalls: Effects of Chemical Bath Deposition Time and Annealing Temperature. Vol. 7, Chemosensors. 2019.
12. Pradhan D, Sindhwani S, Leung KT. Parametric Study on Dimensional Control of ZnO Nanowalls and Nanowires by Electrochemical Deposition. Nanoscale Res Lett. 2010;5(11):1727-36.
13. Rafique S, Han L, Zhao H. Density Controlled Growth of ZnO Nanowall–Nanowire 3D Networks. J Phys Chem C. 2015;119(21):12023-9.
14. Wu CC, Wuu DS, Lin PR, Chen TN, Horng RH. Effects of Growth Conditions on Structural Properties of ZnO Nanostructures on Sapphire Substrate by Metal–Organic Chemical Vapor Deposition. Nanoscale Res Lett. 2009;4(4):377.
15. Tang J-F, Tseng Z-L, Chen L-C, Chu S-Y. ZnO nanowalls grown at low-temperature for electron collection in high-efficiency perovskite solar cells. Sol. Energy Mater Sol. Cells. 2016;154:18-22.
16. Jang E-S. Recent Progress in Synthesis of Plate-like ZnO and its Applications: A Review. J Korean Ceram Soc. 2017;54(3):167-83.
17. Ghai V, Sharma K, Sanger J, Singh H, Agnihotri PK. Ultrafast microwave-assisted synthesis of various zinc oxide nanostructures. Indian J Eng Mater Sci. 2020;27(Apr-2020):365.
18. Ručman S, Intra P, Kantarak E, Sroila W, Kumpika T, Jakmunee J, et al. Influence of the magnetic field on bandgap and chemical composition of zinc thin films prepared by sparking discharge process. Sci Rep. 2020;10(1):1388.
19. Thongsuwan W, Sroila W, Kumpika T, Kantarak E, Singjai P. Antireflective, photocatalytic, and superhydrophilic coating prepared by facile sparking process for photovoltaic panels. Sci Rep. 2022;12(1):1675.

20. Xiao S, Tian S, Cressault Y, Zhang X, Tang J, Li Y, et al. Study on the influence of O2 on the breakdown voltage and self-recovery characteristics of c-C4F8/N2 mixture. AIP Adv. 2018;8(8):85121.
21. ASTM G173-03 Reference Spectra Derived from SMARTS v. 2.9.2 [Internet]. [cited 2023 Aug 12].
22. Shichen S, Xiaodong Y, Candong H. Fabrication of ZnO nanowall-network ultraviolet photodetector on Si substrates. J Semicond. 2011;32(7):74008.
23. Wu W-Y, Ting J-M, Chang C-K. Morphology-selected, room-temperature growth of ZnO nanostructures. CrystEngComm. 2010;12(5):1433-8.
24. Wongsaeng C, Singjai P. Mobilities in ambipolar field effect transistors based on single-walled carbon nanotube network and formed on a gold nanoparticle template. Appl Phys Lett. 2014;104(14).
25. Chang Y-C, Lin Y-R, Chen S-W, Chou C-M. Density-Controlled Growth of ZnO Nanowalls for High-Performance Photocatalysts. Materials (Basel). 2022;15: 9008.
26. Hornyak GL, Tibbals HF, Dutta J, Moore JJ. Introduction to Nanoscience & Nanotechnology. USA: CRC Press, Taylor & Francis Group, LLC; 2009. p. 1205.
27. Knight RD, Jones B, Field S. College Physics A Strategic Approach. USA: Pearson Addison-Wesley; 2007. p. 701.
28. Wongsaeng C. Synthesis and Electronic Analysis of Single-Walled Carbon Nanotube and Metal Nanoparticle Contacts. Chiang Mai University; 2013.
29. Xu Y, Yan X-T. Chemical Vapour Deposition An Integrated Engineering Design for Advanced Materials. Springer Verlag London Limited; 2010. p. 2.
30. Grove AS. Physics and Technology of Semiconductor Devices. USA: John Wiley & Sons, Inc.; 1967. p. 13.
31. Chen Q, Jiang C, Chen M, Zhang J, Hou G, Tang Y. Magnetic field stabilizes zinc anode. Surfaces and Interfaces. 2022;31:101972.

